

The role of stellar relaxation in the formation and evolution of the first massive black holes

Hidenobu Yajima^{1,2*} and Sadeh Khochfar³

¹ *Frontier Research Institute for Interdisciplinary Sciences, Tohoku University, Sendai 980-8578, Japan*

² *Astronomical Institute, Tohoku University, Sendai 980-8578, Japan*

³ *SUPA†, Institute for Astronomy, University of Edinburgh, Royal Observatory, Edinburgh, EH9 3HJ, UK*

Accepted ?; Received ??; in original form ???

ABSTRACT

We present calculations on the formation of massive black holes with $10^5 M_\odot$ at $z > 6$ that can be the seeds of supermassive black holes at $z \gtrsim 6$. Under the assumption of compact star cluster formation in merging galaxies, star clusters in haloes of $10^8 \sim 10^9 M_\odot$ undergo rapid core-collapse leading to the formation of very massive stars (VMSs) with $\sim 1000 M_\odot$ which directly collapse into black holes with similar masses. Star clusters in halos of $\gtrsim 10^9 M_\odot$ experience type-II supernovae before the formation of VMSs due to long core-collapse time scales. We also model the subsequent growth of black holes via accretion of residual stars in clusters. 2-body relaxation efficiently re-fills the loss cones of stellar orbits at larger radii and resonant relaxation at small radii is the main driver for accretion of stars onto black holes. As a result, more than ninety percent of stars in the initial cluster are swallowed by the central black holes before $z = 6$. Using dark matter merger trees we derive black hole mass functions at $z = 6 - 20$. The mass function ranges from 10^3 to $10^5 M_\odot$ at $z \lesssim 15$. Major merging of galaxies of $\gtrsim 4 \times 10^8 M_\odot$ at $z \sim 20$ successfully leads to the formation of $\gtrsim 10^5 M_\odot$ BHs by $z \gtrsim 10$ which can be the potential seeds of supermassive black holes seen today.

Key words: radiative transfer – ISM: dust, extinction – galaxies: evolution – galaxies: formation – galaxies: high-redshift

1 INTRODUCTION

Recent observations of high-redshift QSOs at $z > 6$ suggest supermassive black holes (SMBH) of $M_{\text{BH}} \gtrsim 10^9 M_\odot$ form on short time scale $\lesssim 1$ Gyr (e.g., Fan et al. 2001, 2006; Mortlock et al. 2011; Kormendy & Ho 2013; Wu et al. 2015). The most distant QSOs are observed at $z = 7.1$ which corresponding to an age of the Universe of ~ 800 Myr. The formation mechanism of SMBHs on such short time scales has not been understood yet. Cosmological simulations show that BHs can grow up to $\sim 10^9 M_\odot$ via Bondi-Hoyle accretion (Di Matteo et al. 2008, 2012; Li et al. 2007). While there are uncertainties associated with the modelling of the accretion efficiency at the sub-grid level (Booth & Schaye 2009), it appears that the main crucial assumption is that massive black holes (MBHs) of $10^5 M_\odot$ are seeded in haloes of $\sim 10^{10} M_\odot$ within the simulations. These simulations indicate that once MBHs form in the first galaxies, they can

grow to SMBH via gas accretion at Eddington rate by $z \sim 6$. The main obstacle is thus referred to forming MBHs.

One natural scenario for the formation of massive BHs is the Eddington-limited growth of a few $100 M_\odot$ stellar mass black hole via gas accretion that is the remnant of a Population III star. However, due to stellar feedback, the gas accretion rate is significantly suppressed and far below the Eddington-limit (Milosavljević et al. 2009b,a; Alvarez et al. 2009; Park & Ricotti 2011, 2012). In addition, cosmological simulations show that Population III star remnants mostly resided in low-density environments, hence the gas accretion rate is much smaller than the Eddington rate even without stellar feedback (Alvarez et al. 2009).

Another proposed mechanism is the direct collapse of super massive stars (SMS) (Rees 1978; Bromm & Loeb 2003). If the formation of hydrogen molecules in the first galaxies is suppressed by external UV radiation in the Lyman-Werner bands, gas clouds cannot fragment. As a result, the clouds cannot form low mass stars but form SMSs of $\sim 10^5 M_\odot$ due to high-gas accretion rates of $\sim 0.1 - 1.0 M_\odot \text{ yr}^{-1}$ (Omukai et al.

* E-mail: yajima@astr.tohoku.ac.jp (HY)

† Scottish Universities Physics Alliance

2005; Lodato & Natarajan 2006, 2007; Begelman et al. 2006; Spaans & Silk 2006; Inayoshi & Omukai 2012; Agarwal et al. 2012, 2013; Hosokawa et al. 2013). This scenario is also supported by detailed numerical simulations (Regan & Haehnelt 2009; Regan et al. 2014; Mayer et al. 2010; Choi et al. 2013; Latif et al. 2013; Johnson et al. 2014; Inayoshi et al. 2014; Agarwal et al. 2014). One of the main requirements of this scenario is a strong UV background radiation with $J_{21} \gtrsim 100$ in units of $10^{-21} \text{ erg s}^{-1} \text{ cm}^{-2} \text{ Hz}^{-1}$ and very low metallicity ($Z \lesssim 10^{-5} Z_{\odot}$) (Omukai et al. 2005, 2008; Dijkstra et al. 2008; Agarwal & Khochfar 2015; Sugimura et al. 2014; Inayoshi & Tanaka 2014).

Recently Mayer et al. (2010) showed in high-resolution simulations that another suggested path to the formation of MBHs via major mergers of galaxies could work. Their simulations showed that a large amount of gas in disc galaxies falls down to the galactic centres due to angular momentum loss by tidal force, and massive high-density gas clumps form. They suggest that the gas clouds directly collapse into MBHs.

In addition, Inayoshi et al. (2015) suggested that SMSs could form in merging primordial haloes due to collisional dissociation of H_2 in the compressed high-density regions. The outcome of the collapse depends sensitively on the equation of state of the gas. If radiative cooling quickly occurs, a collapsing gas cloud fragments and forms a dense star clusters instead (e.g., Regan & Haehnelt 2009; Ferrara et al. 2013).

In such dense star clusters MBHs form due to interactions between stars and BHs via a series of stellar merging and tidal disruption events (e.g., Rees 1978). Direct numerical simulations by Portegies Zwart & McMillan (2002) support this view and show that compact dense star clusters cause core-collapse and make very massive stars (VMSs) of $\sim 1000 M_{\odot}$ within the typical lifetime of massive stars (see also, Fujii & Portegies Zwart 2014).

Very recently Katz et al. (2015) followed the merging processes of metal enriched haloes in detailed cosmological hydrodynamics simulations and showed the formation of high-density gas clumps which are potential sites of dense star clusters leading to the formation of VMSs. In this work, we investigate the possibility of the formation of MBHs via the formation of VMSs and subsequent growth by stellar relaxation processes in merging galaxies at $z > 6$.

Our paper is organized as follows. We describe our model in Section 2. In Section 3, we show the masses of VMSs as a function of halo mass, and the final BH masses, and the mass function of MBHs. In Section 4, we investigate the effects of Population III stars and the nature of metal poor globular clusters. Finally, in Section 5, we summarize our main conclusions.

2 MODEL

The starting point of our model is the formation of compact star clusters in major mergers ($M_1/M_2 < 3.5$, $M_1 \geq M_2$) of gas-rich disc galaxies. It has been shown in a series of numerical simulations that during such events gas initially in a rotationally supported disc loses angular momentum and collapses toward the potential minimum of the merger remnant (Barnes & Hernquist 1996; Springel et al. 2005;

Di Matteo et al. 2005; Naab et al. 2006; Hopkins et al. 2006; Cox et al. 2006; Li et al. 2007; Mayer et al. 2010). This gas will reach high densities on short time scales and be available to fuel star formation in the centre. The low amount of angular momentum facilitates the formation of compact star clusters (Regan & Haehnelt 2009).

The progenitor disc is assumed to relate to the hosting dark matter halo via $R_d \sim \lambda R_{\text{vir}}$ (e.g., Mo et al. 1998), where λ and R_{vir} are spin parameter and virial radius, respectively. In this work, we assume $\lambda = 0.05$, however, our results are not depending on the specific choice of λ as we will show below.

We model the progenitor discs of merging galaxies as a Mestel, isothermal profile, i.e., $\Sigma(r) = \Sigma_0(R_d/r)$, where Σ_0 and R_d are scale parameters and estimated as a function of halo properties (Mo et al. 1998; Devecchi et al. 2010),

$$\begin{aligned} \Sigma_0 &= 70 \left(\frac{V_h}{15 \text{ km s}^{-1}} \right) M_{\odot} \text{ pc}^{-2}, \\ R_d &= 100 \left(\frac{\lambda}{0.05} \right) \left(\frac{R_{\text{vir}}}{700 \text{ pc}} \right) \text{ pc}. \end{aligned} \quad (1)$$

Here V_h is the circular velocity.

The amount of inflowing gas during the merger is estimated using the prescription in Hopkins et al. (2009), which assumes that during the merger a gaseous and stellar bar develop which are out of sync and exert a torque on each other. The resulting mass inflow of gas is then estimated by,

$$M_{\text{inf}} = 2\pi \Sigma_0 R_d V_h (1 - f_{\text{gas}}) f_{\text{disc}} \Psi_{\text{bar}} \Delta\tau, \quad (2)$$

where f_{gas} is the gas fraction in the disc, f_{disc} is the fraction of the disc mass to the total mass including bulge and dark matter ($\sim \lambda$: van den Bosch 2001), Ψ_{bar} is the mass fraction of stars in the bar, and $\Delta\tau$ is the time since the merger. We assume $f_{\text{gas}} = 0.9$, i.e., 10% of the disc is in stars before the merger takes place. The mass of the resulting star cluster increases with decreasing f_{gas} , leading to formation of more massive BHs as we will show below. As suggested in Hopkins et al. (2009), we set $\Psi_{\text{bar}} = 1$.

We consider the initial 3 Myr after the merger, which corresponds to the life time of massive stars and the onset of supernovae feedback which will halt star formation in the star cluster.

Once mass inflow occurs the inner structure of the disc will change. However, we here focus on regions at galactic centres that are much smaller than these scales and we assume that the gas distribution is spherical. Prior to star formation we approximate the density profile of the central clouds with a singular isothermal profile,

$$\rho_{\text{gas}} = \frac{c_s^2}{2\pi G r^2} \quad (3)$$

where c_s is the sound speed which we approximate using the virial temperature of the hosting halo. Recent simulations by Katz et al. (2015) support the assumption of central high-density gas clumps formed during galaxies mergers with r^{-2} profiles. By integrating the density profile, we determine the radius of star clusters, i.e., $M_{\text{inf}} = \int_0^{r_{\text{cl}}} 4\pi r^2 \rho_{\text{gas}} dr$, hence,

$$r_{\text{cl}} = 0.22 \text{ pc} \left(\frac{c_s}{10 \text{ km s}^{-1}} \right)^{-2} \left(\frac{M_{\text{inf}}}{10^5 M_{\odot}} \right). \quad (4)$$

In general, the star formation rate in such gas cloud can be parameterised by $\dot{M}_{\text{star}} \sim \eta \frac{M_{\text{gas}}}{t_{\text{dyn}}}$ where $\eta \lesssim 0.05$ is

the star formation efficiency (e.g., Krumholz et al. 2012). The dynamical time of the gas clouds in our model is typically $\lesssim 10^4$ yr which is much shorter than 3 Myr. Therefore, we assume the fiducial case of $M_{\text{cl}} \sim M_{\text{inf}}$. On the other hand, before supernovae occurs, radiative feedback may reduce the conversion efficiency from gas to stars due to photo-evaporation of gas. Hence, we also study the case of $M_{\text{cl}} = 0.3M_{\text{inf}}$.

The star clusters undergo core-collapse, and massive stars migrate toward the centre of the star cluster. Recent N-body simulations show that the time scale of core-collapse is similar to that of dynamical friction (Fujii & Portegies Zwart 2014),

$$t_{\text{CC}} \sim t_{\text{df}} = \frac{1.91}{\ln(\Lambda)} \frac{r_{\text{cl}}^2 \sigma}{G m_{\text{max}}} \quad (5)$$

where $\ln(\Lambda)$ is the Coulomb logarithm, σ is the velocity dispersion of stars and m_{max} is the maximum mass of stars based on the initial stellar mass spectrum. We assume that the stellar cluster is that of a King profile and use a Salpeter initial mass function with the mass range of $m = 0.1 - 100 M_{\odot}$. Due to core-collapse, the stellar density at the centre quickly rises. As a result, at the centre, stars frequently collide with each other and coalesce, resulting in the formation of very massive stars (VMSs) of $\sim 1000 M_{\odot}$ (Portegies Zwart & McMillan 2002). Numerical simulations estimate the final mass of such VMS as (Portegies Zwart & McMillan 2002):

$$M_{\text{VMS}} = m_{\text{max}} + 4 \times 10^{-3} M_{\text{cl}} f_c \ln(\Lambda) \ln \left(\frac{3 \text{ Myr}}{t_{\text{CC}}} \right) \quad (6)$$

where M_{cl} is the mass of the star cluster, and f_c is the factor used to calibrate the analytical estimate against direct N-body simulations ($f_c = 0.2$; Portegies Zwart & McMillan 2002).

If the core-collapse time scale t_{CC} is longer than 3 Myr, stars will explode as type-II supernovae and we set $M_{\text{VMS}} = m_{\text{max}}$. Following Portegies Zwart & McMillan (2002) and Fujii & Portegies Zwart (2014), we use a King profile with $W_0 = 3$ for the stellar density distribution of our model star clusters. If the mass of the VMSs are greater than $\sim 260 M_{\odot}$, VMSs directly collapse to BHs (Heger & Woosley 2002). After core-collapse, star clusters can shrink by a factor of a few (Fujii & Portegies Zwart 2014), massive stars tend to distribute near the centres of star clusters due to mass segregation. We here will use the initial state of the star cluster in our calculations, noting that the calculated growth rates will be lower limits based on the fact that we do not take into account core collapse and mass segregation in the cluster. Subsequent disruptions of stars by the BH deplete the loss cone and drive the growth of the BH to a halt. However, the loss cone can be refilled by stars that loose angular momentum and migrate towards the centre or have a high ellipticities. In this work, we consider angular momentum transport due to relaxation processes between stars. We will focus on two main types of relaxation processes, *resonant* and *non-resonant*.

Two-body relaxation (non-resonant:NR) takes place over a time scales of (e.g., Binney & Tremaine 2008; Kocsis & Tremaine 2011),

$$t_{\text{NR}}(r) = 0.34 \frac{\sigma^3}{G^2 \rho m_2 \ln(\Lambda)}, \quad (7)$$

where ρ is the stellar density, and $m_2 = \langle m^2 \rangle / \langle m \rangle$ is the effective mass. For a Salpeter IMF in the mass range $0.1 - 100 M_{\odot}$, $m_2 = 4.8 M_{\odot}$.

The second relaxation process we consider is resonant relaxation (RR). Stars close to MBH move on Kepler orbits. These stars cause wire-like fluctuation in the gravitational potential governed by the MBH, and induce perturbations to stellar orbits. In particular, stars on the same plane exchange angular momentum via scalar RR resulting in a change of ellipticities of the orbits. As a result, stars with high ellipticity enter within the tidal radius of the central MBH and will be disrupted by it. The effect of scalar RR can be suppressed by Newtonian and general relativistic precession (Hopman & Alexander 2006), in contrast to the classical Keplerian case.

The scalar RR time scale is estimated by (Hopman & Alexander 2006),

$$t_{\text{RR}}^s(r) = \frac{A_{\text{RR}}}{N(<r)} \left(\frac{M_{\text{BH}}}{\bar{m}} \right)^2 P^2(r) \left| \frac{1}{t_{\text{M}}} - \frac{1}{t_{\text{GR}}} \right|, \quad (8)$$

where A_{RR} is a numerical factor of order unity (~ 3.56 ; Rauch & Tremaine 1996), \bar{m} is a mean stellar mass, $P(r) = 2\pi[r^3/(GM_{\text{BH}})]^{1/2}$, t_{M} and t_{GR} are the Newtonian and general relativistic precession time scales. Following Hopman & Alexander (2006), we estimate the Newtonian and general relativistic precessions as follows, $t_{\text{M}} = A_{\text{M}} \frac{M_{\text{BH}}}{N(r)\bar{m}} P(r)$, and $t_{\text{GR}} = \frac{8}{3} \left(\frac{cJ}{4GM_{\text{BH}}} \right)^2 P(r)$, where $A_{\text{M}} = 1$ is assumed. The shorter of the two relaxation time scales is used to estimate the loss cone refilling and growth of BHs,

$$t_{\text{relax}}(r) = \min(t_{\text{NR}}, t_{\text{RR}}^s). \quad (9)$$

At radii where the interior mass is dominated by the stars and not the BH we only consider t_{NR} , because the stellar orbits are not Keplerian anymore. Over the relaxation time scale T_{relax} , the angular momentum of stars is transported, and hence, the loss-cone is refilled, causing the growth of BHs. We estimate the BH mass by integrating the stellar density profile and time evolution as follows (see also Chen & Liu 2013),

$$M_{\text{BH}}(t) = M_{\text{BH}}^{\text{init}} + \int_0^t dt \int_0^{r_{\text{cl}}} \frac{4\pi r^2 \rho_{\text{star}}(r, t)}{t_{\text{relax}}(r, t)} dr. \quad (10)$$

3 RESULTS

3.1 Formation of very massive stars

Figure 1 shows the predicted mass of VMSs based on Eq. 6 as a function of the halo mass of the remnant. Most notably the mass of VMSs drops beyond halo masses of $M_{\text{h}} \sim 10^{8.5-9}$. This is a direct consequence of the increasing core collapse time scale t_{CC} in larger haloes. The difference in predicted masses of VMSs as a function of redshift is again related to the longer core-collapse time scales at low redshifts, which result in systematic lower masses. Once the core collapse time scale is larger than the life time of massive stars, i.e. 3 Myr, we assume that collisions between stars become negligible during the life-time of the star, and no VMS is formed. The long relaxation times would even in the case that a remnant black hole forms, be too long to grow it efficiently. The mass of VMSs increases with halo mass, because the

mass of star clusters increases with halo mass in our model. However, with increasing cluster mass and radius, the core-collapse time becomes longer too. The mass growth of VMSs is logarithmic and only weak until $t_{\text{CC}} \sim 3$ Myr. Haloes with $M_h \sim 10^9 M_\odot$ at $z \gtrsim 20$ can host VMSs of $\sim 1000 M_\odot$. Note that, in this work, we assume low stellar metallicities ($Z \lesssim 10^{-3} Z_\odot$). If stellar metallicities are higher than $Z \gtrsim 10^{-3} Z_\odot$, stars experience strong stellar winds and lose a large fraction of their mass before their death. The maximum mass of VMSs increases with redshift from $290 M_\odot$ for a halo of $1.1 \times 10^8 M_\odot$ at $z = 7$ to $1200 M_\odot$ for a halo of $6.7 \times 10^8 M_\odot$ at $z = 20$. In our model, M_{cl} for a specific halo mass does not depend on redshift, because in Equation 2, $\Sigma_0 \propto (1+z)^{1/2}$, $V_h \propto (1+z)^{1/2}$, and $R_{\text{vir}} \propto (1+z)^{-1}$. On the other hand, $R_{\text{cl}} \propto (1+z)^{-1}$, hence star clusters become bigger with decreasing redshift.

As a result, the core-collapse time becomes longer, and the mass of VMSs decreases. If the stellar metallicity is low, even $\sim 100 M_\odot$ stars can directly collapse into BHs (Heger et al. 2003). Feedback by supernovae can suppress further gas accretion or evacuate gas from galaxies.

Once gas is evacuated from the disc and becomes part of the hot diffuse halo, it will take a cooling time, for it to join the disc again. Here we roughly estimate the feedback necessary to unbind the gas from the disc. The feedback energy by SNe is $E_{\text{SN}} \sim 0.007 \left(\frac{M_{\text{cl}}}{M_\odot} \right) \times 10^{51}$ erg, where 0.007 is the conversion factor from the star cluster's mass to number of massive stars causing type-II SNe given a Salpeter IMF in the mass range $0.1 - 100 M_\odot$. From Equation (2), $E_{\text{SN}} \propto M_h$. The disc binding energy is $E_{\text{grav}} \sim \frac{GM_d^2}{R_d} \propto \frac{M_h^2}{R_{\text{vir}}}$. Then, $E_{\text{SN}}/E_{\text{grav}} \propto R_{\text{vir}} \propto (1+z)^{-1}$. Hence gas in discs can easily be evacuated at lower redshift, due to its lower density. The threshold mass for haloes with $E_{\text{grav}} > E_{\text{SN}}$ is $M_h \gtrsim 1.6 \times 10^9 \left(\frac{1+z}{11} \right)^{1.5}$.

As shown in the figure 1, haloes of $M_h \sim 10^{7.5} - 10^9 M_\odot$, which are in the typical mass range of the first galaxies (Wise et al. 2012b; Johnson et al. 2013; Paardekooper et al. 2013), form compact star clusters and cause the formation of VMSs. The VMSs of haloes with $M_h \lesssim 10^{7.5} M_\odot$ result in pair-instability SNe (Heger et al. 2003).

3.2 Growth of BHs

Once a VMS of $> 260 M_\odot$ is formed collapse to a BH will ensue in a star cluster. In such a system RR/NR efficiently changes the angular momentum of stars, and refills the loss cone around the BH allowing it to feed. Figure 2 shows the RR and NR time scale as a function of radial distance from the centre of a star clusters. Due to general relativistic precession a shortest time scale exists at a specific position. For a star cluster with $M_{\text{cl}} = 10^5 M_\odot$ and $R_{\text{cl}} = 0.25$ pc which is representative of the result of a merger between proto-galaxies with $M_h = 3.8 \times 10^8 M_\odot$ at $z = 15$, the NR time scale becomes shorter than RR at $r \lesssim 0.02$ pc.

Hence, RR efficiently works for stellar accretion near the BH, and NR leads to the angular momentum change of stars in the outer parts.

As the stellar density decreases with time, the relaxation time scale becomes longer. The RR and NR time scales at $t = 1$ Myr are shown as the dash lines in the figure. The time scales get longer by a factor $\gtrsim 2$ from the initial state.

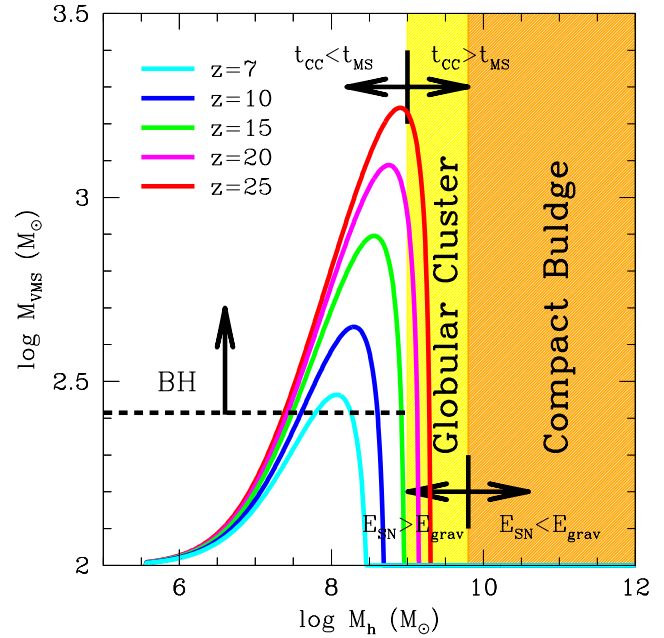


Figure 1. Mass of very massive stars in star clusters after core-collapse. Different colour lines represent different redshifts at which galaxies merge. Dashed line shows the threshold mass of stars that result in black holes at end of their life time (Heger et al. 2003).

The radius at which the RR time scale becomes shorter than the NR propagates outwards with time. In the fiducial case shown in figure 2 the radius is 0.1 pc at $t = 1$ Myr. Finally, depending on the RR and NR processes, the time scale for refilling of the loss cone can be shorter than $\sim 10^8$ yr in the clusters.

Following Equation 10, the stellar density at a specific radius decreases with time due to RR and NR processes. Figure 3 shows the time evolution of the stellar density profile. Stars at $r \sim 10^{-3}$ pc have short RR relaxation time scales and are quickly consumed by the central BH, which in turn generates a density gap. Stars close to the gap will be accreted next onto the BH. Initially the radius at which the total enclosed stellar mass is smaller than the central BH, is limited to $r \lesssim 10^{-3}$ pc at $t \sim 10^7$ yr, therefore, all stars at large radii are only affected by NR. As the BH grows, the radius at which RR dominates becomes larger and reaches the radius of the cluster at $t \sim 10^8$ yr.

We follow the time evolution of the BH growth from the merging event till redshifts $z = 6$. The distribution of BH masses is shown in Figure 4. As shown in Figure 1, only haloes in the limited mass range ($M_h \sim 10^7 - 10^9 M_\odot$) contribute to the formation of MBH seeds.

As equation 7 shows, the NR time scale is proportional to the stellar velocity dispersion and the inverse of stellar mass density. Since the stellar density is almost constant despite of the cluster's mass in our model, the BH growth rate is high even in low mass haloes or stellar clusters. However, as it will be show below, most of the stars even in massive star clusters accrete onto a central BH by $z = 6$. Hence, the BH mass linearly increases with halo mass. We also compare the case without NR for galaxies that merge

at $z = 20$, shown as the magenta dash line in the figure. Unlike in the case of both RR and NR processes active, the BH mass without NR is almost independent of halo mass, and smaller than that with NR.

The radial dependence of the RR time scale implies that at small radii fast accretion of material onto the black hole will occur stalling the growth of the black hole until further material from larger radii is transported inwards. In the absence of NR the transport of material from larger radii is very inefficient in effect limiting the black hole mass in our model to $\sim 10^4 M_\odot$. Thus NR is able to tap into the mass budget of stellar clusters at large radii and RR efficiently funnels this material close to the black hole for accretion.

Figure 5 shows the conversion fraction of the initial stellar mass of a cluster into a MBH by $z = 6$. As shown in Figure 2, the relaxation time scale is shorter than the average duration from the first merging event to $z = 6$, hence most of the stars (\gtrsim ninety per cent) accrete onto a central BH. With decreasing stellar density, the NR time scale gets longer, resulting in slow BH mass growth. The position at which the NR time scale becomes shortest gets closer to R_{cl} as the cluster mass decreases, resulting in smaller conversion factors of stars in clusters with $\gtrsim 10^5 M_\odot$. In addition, as the stellar velocity dispersion increases with the star cluster's mass, the NR time scale becomes longer, resulting in a somewhat inefficient conversion factor.

In order to study the efficiency of stellar mass accretion, we compare it with the Eddington rate. Figure 6 represents the time averaged mass accretion rate normalized to the Eddington rate. The mass accretion rate increases with redshift, because star clusters are more compact and the relaxation time scale becomes shorter for mergers at higher redshift in our model.

Due to the short relaxation timescale, the clusters lose most of their stars before $z = 6$. After most of the stars are swallowed, the stellar accretion rate rapidly decreases as shown in Figure 2. Therefore, the Eddington ratio at $z \geq 15$ is lower than that at $z \leq 10$.

However, even for star clusters formed at $z = 25$, the time average accretion rate is close to the Eddington rate ($\dot{M}/\dot{M}_{Edd} \sim 0.5$). In addition, at $M_h \sim 10^9 M_\odot$, the accretion increases steeply. As shown in Figure 1, the initial BH (VMS) mass sharply drops at $M_h \sim 10^9 M_\odot$ due to the longer core-collapse timescale. On the other hand, the NR timescale is independent of the central BH mass. Hence, the Eddington ratio in the initial phase is very high.

Thus, we suggest that the stellar accretion can be the dominant mode for the growth of BHs up to a mass of $\sim 10^5 M_\odot$. For further growth of BHs to $\sim 10^9 M_\odot$, efficient gas accretion is required.

3.3 Number density of seeds of massive BHs

To estimate the cosmological relevance of the above discussed formation channel, we combine our analytic model with a Monte-Carlo technique based dark matter merger tree. In combination with the dark matter mass function at any given redshift this will allow to predict the merger rate of galaxies and the associated black hole mass function (BHMF).

Merger trees are constructed and applied based on the extended Press-Schechter formalism (Lacey & Cole

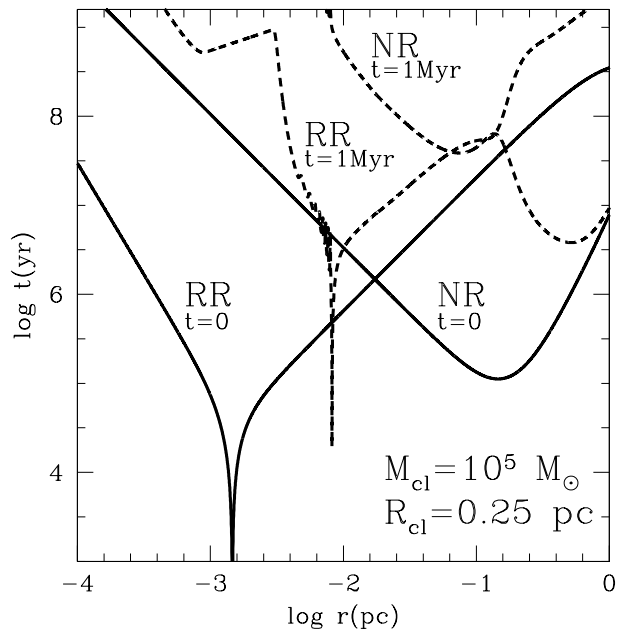


Figure 2. Time scales of stellar relaxation processes as a function of radial distance from centre of a star cluster. NR and RR represent non-resonant relaxation (2-body) and resonant relaxation. Solid and dash lines show the relaxation time scale at $t = 0$ and 1 Myr, respectively. The time scales are calculated for a star cluster with the mass of $10^5 M_\odot$ and the radius of 0.25 pc.

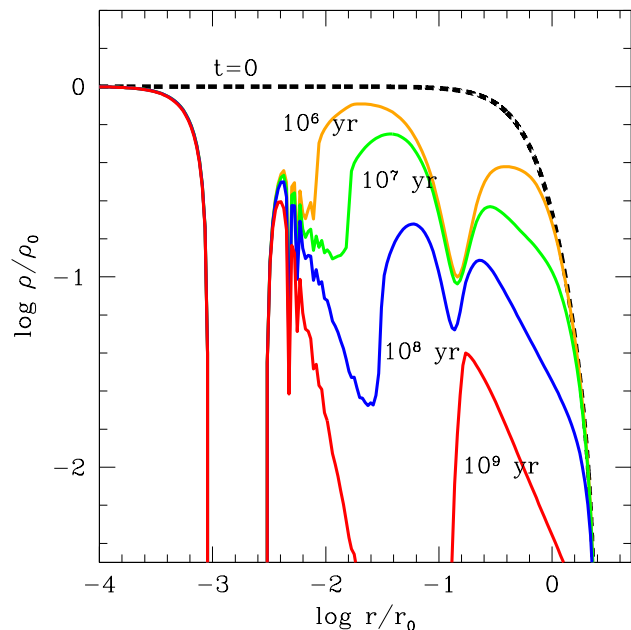


Figure 3. Radial stellar density profiles. Different colours show the stellar density at different evolution times. The time scales are calculated for a star cluster with the mass of $10^5 M_\odot$ and radius of 0.25 pc.

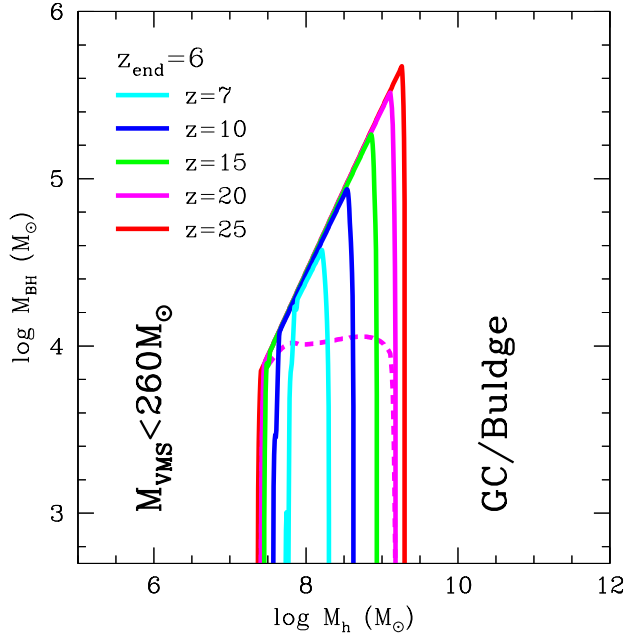


Figure 4. Black hole mass as a function of galaxy mass at $z = 6$. Different colour lines represent different redshifts at which galaxies merge. The magenta dashed-line is the black hole mass without 2-body relaxation for clusters formed at $z = 20$.

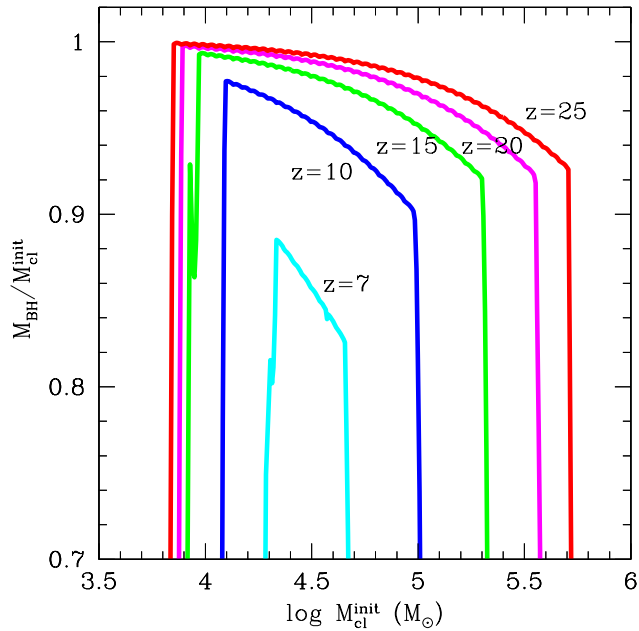


Figure 5. Final BH mass at $z = 6$ normalized by the initial star cluster's mass. Different colour lines represent different formation redshifts of the star clusters.

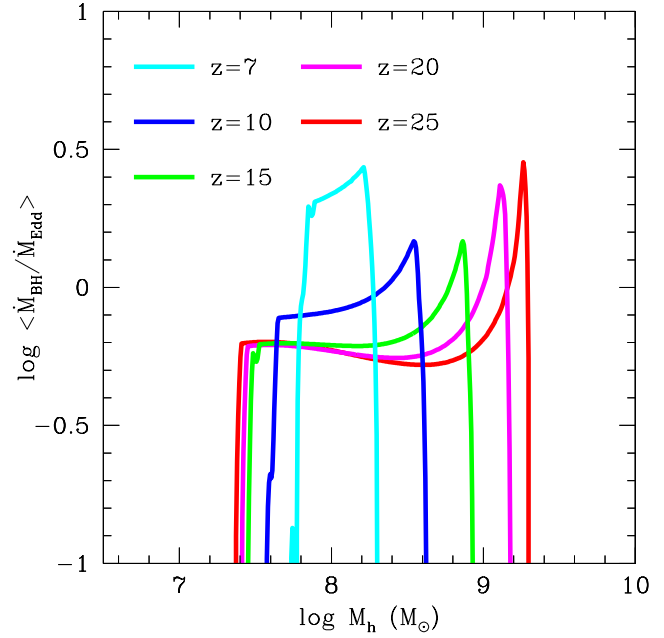


Figure 6. Time-averaged stellar accretion rate normalized by the Eddington rate. Different color lines represent different redshifts at when galaxies merge.

1993) using the algorithm presented in Somerville & Kolatt (1999). The merger trees have been successfully implemented and tested in previous work (e.g., Khochfar & Silk 2009, 2011). Our sample consists of 1000 merger tree realisations for each individual dark halo mass bin ($10^8 M_\odot$ to $10^{13} M_\odot$). Each tree is resolved down to a minimum halo mass of $10^7 M_\odot$. We use cosmological parameters based on WMAP9 (Hinshaw et al. 2012), $\Omega_\Lambda = 0.7$, $\Omega_M = 0.3$, $\sigma_8 = 0.9$ and $h = 0.7$.

Figure 7 shows the redshift evolution of six sampled haloes which reach the halo mass of $10^8, 10^9, 10^{10}, 10^{11}, 10^{12}$ and $10^{13} M_\odot$ at $z = 6$ respectively. The yellow shade region represents the mass range in which the merging haloes can form MBH seeds. As seen in the Figure and expected, massive haloes experience mergers in the shaded region at higher redshifts. For example, most haloes with $M_h \geq 10^{12} M_\odot$ at $z = 6$ can form MBH seeds at $z \gtrsim 15$, resulting in plausible seeds of SMBHs at $z \gtrsim 6$. In addition, due to the variation in the redshift when the actual merger occurs, haloes with the same mass at $z = 6$ can host MBHs of different mass.

Major mergers with mass ratio $\lesssim 1 : 3$ are effective means in transporting angular momentum and allowing the gas to collapse to the central region of a galaxy (e.g. Bois et al. 2010). The efficiency of this process decreases with increasing mass ratio and we will in the following focus only at major mergers with mass ratio $< 1 : 2$. We have checked that inclusion of minor mergers does not change the BHMF significantly. We identify the first major merger event in the history of a halo as the BH seeding event.

Figure 8 shows the predicted BHMFs at $z = 6, 10, 15$ and 20 . At $z = 20$, the BHMF is limited to $M_{BH} \lesssim 10^4 M_\odot$ because the merging events just took place. As time pro-

gresses the number density of BHs and their average mass increases.

At $z \sim 10 - 15$ we find MBHs of $\sim 10^5 M_\odot$ with number densities of $\sim 10^{-6}$ to 10^{-7} Mpc^{-3} . If we assume $M_{\text{cl}} = 0.3M_{\text{inf}}$, the number densities decrease to $\sim 10^{-8}$ to 10^{-9} Mpc^{-3} which are similar to that of observed QSOs at $z \gtrsim 6$ (e.g., Fan et al. 2006). This is because the core-collapse time scale gets longer, hence the halo mass range becomes narrower. In addition, the growth rate of MBHs by stellar relaxation also becomes lower.

MBHs of $10^5 M_\odot$ that grow close to the Eddington limit will reach $\sim 10^9 M_\odot$ by $z \sim 6 - 7$ and thus could be the potential progenitors. To illustrate this point, one can consider a MBH formed at $z = 15$ (10), it can reach $10^9 M_\odot$ at $z = 6$ with an average Eddington rate of 0.6 (0.9).

Cosmological simulations show that $10^5 M_\odot$ MBHs at galactic centres can grow to $\sim 10^9 M_\odot$ by $z \sim 6$ via gas accretion using a the Bondi-Hoyle model at the sub-grid level (e.g., Di Matteo et al. 2005, 2012; Li et al. 2007). These simulations show that once a MBH is formed at the centre of galaxies in the halos with $M_h \gtrsim 10^{10} M_\odot$, the gas keeps accreting onto the MBH close to the Eddington limit even under the presence of feedback (see however, Johnson & Khochfar 2011, for high resolution simulations including radiative transfer.). If we allow the MBH seeds of $10^5 M_\odot$ to grow at the Eddington limit, the time needed to grow from 10^5 to $10^9 M_\odot$ is $t = \frac{\epsilon}{1-\epsilon} \tau_{\text{Sal}} \ln 10^4 \sim 0.46 \text{ Gyr}$ for $\epsilon = 0.1$, where τ_{Sal} is the Salpeter time scale $= \frac{c\sigma_T}{4\pi G m_p}$. Hence, in order to explain SMBHs of $10^9 M_\odot$ at $z \sim 6$ (7), MBH seeds of $10^5 M_\odot$ are required at $z \gtrsim 10$ (13). Our models satisfy these constraint.

It is well known observationally that the mass of MBHs at galactic centres in local galaxies tightly correlates with the stellar mass of galactic bulges (e.g., Marconi & Hunt 2003; Gültekin et al. 2009). On the other hand, at high redshifts, the BH-stellar mass relation is less well constraint, due to difficulties of observing BHs of $\lesssim 10^8 M_\odot$. Here, using recent observational results of stellar mass densities (Stark et al. 2013), we compare our modelled BH mass density to the stellar mass density. Figure 9 shows the cumulative BH mass per unit volume. Due to the increase in the number density of haloes having masses of $\sim 10^{7.5} - 10^9 M_\odot$ and the growth of BH masses, the cumulative BH mass increases with decreasing redshift. The predicted BH mass density is approximately 5 orders of magnitude smaller than the observed stellar mass density at $z \sim 10$, and continues to become even smaller with respect to the stellar mass density. This can be attributed to not including the effect of gas accretion onto our BH seeds in the model. High gas fractions in high-redshift galaxies mainly maintained by short cooling times are able to support star formation and black hole growth (e.g., Khochfar & Silk 2011). As for the future evolution, any scatter in the BH mass bulge mass relation at early times will reduce and tend toward the observed relation at $z = 0$ due to continued mergers of galaxies and the central-limit theorem (Peng 2007; Hirschmann et al. 2010).

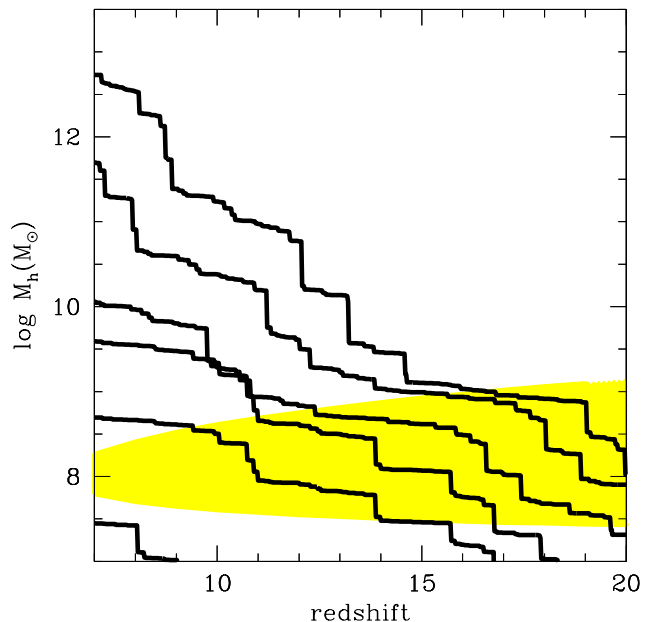


Figure 7. Example redshift evolution of haloes. The yellow shaded region indicates the mass range in which haloes can form BH seeds when they experience major merging.

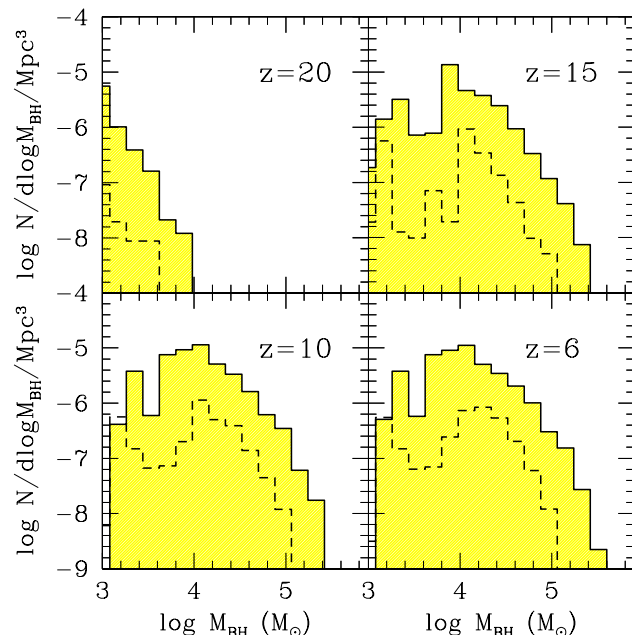


Figure 8. Black hole mass function at $z = 20, 15, 10$ and 6 . Solid and dash lines represent the case of $\epsilon_{\text{SF}} = 1$ (our fiducial model) and 0.3 , where ϵ_{SF} is the conversion efficiency from gas to stars in the inner region $r < r_{\text{cl}}$.

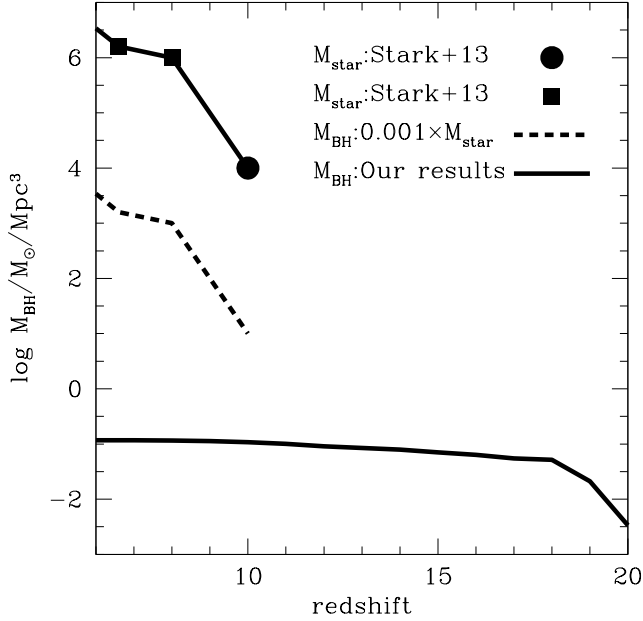


Figure 9. Mass density of stars or black holes in a comoving unit volume of Mpc^3 as a function of redshift. Square and circle symbols show observed stellar mass densities by Stark et al. (2013) and Oesch et al. (2014) respectively. Dashed lines show black hole masses derived by multiplying 10^{-3} to the observed stellar mass densities. The solid line is our result.

4 DISCUSSION

4.1 Population III star cluster

In this work, we consider a Salpeter IMF in the mass range $0.1 - 100 M_\odot$. The initial mass function of metal poor Population III (Pop III) stars is still unknown due to missing observational probes as well as uncertainties in the modelling of their formation. Given that accretion rates onto proto-stellar seeds in primordial gas clouds are high it is generally argued that Pop III stars should be more massive than their metal enriched counterparts (e.g., Omukai & Nishi 1998; Omukai & Palla 2003; Nakamura & Umemura 2001; Bromm et al. 2002; Abel et al. 2002; Yoshida et al. 2006, 2008; Turk et al. 2009; Stacy et al. 2010, 2012; Clark et al. 2011; Umemura et al. 2012; Hirano et al. 2014; Susa 2013; Susa et al. 2014). We re-examine our model trying to account for such massive Pop III stars assuming a top heavy IMF from $10 - 500 M_\odot$ (Hirano et al. 2014) and a slope $\alpha = -2.35$. The resulting BHMF at $z = 6$ is shown in Figure 10. In contrast to star clusters with a fiducial IMF star clusters with a top-heavy IMF produce more massive black holes at their centre per unit mass in stars. Massive Pop III stars cause core-collapse of more massive haloes within 3 Myr, and lead to the formation of heavier VMSs. In addition, because of the increase of the average stellar mass $\langle m \rangle$ from $0.3 M_\odot$ for the normal IMF to $30 M_\odot$ for the Pop III IMF, the relaxation time scale becomes shorter by factor ~ 10 (Equation 7 and 8). As a result, massive BHs of $\gtrsim 10^6 M_\odot$ can form by $z \sim 6$.

In other words, for such a top heavy IMF, even star clusters with similar size and density of typical globular clus-

ters in the local universe can cause core-collapse, and form VMSs.

Note that, however, that massive galaxies ($\gtrsim 10^8 M_\odot$) are likely metal enriched due to type-II SNe of prior stars (e.g., Maio et al. 2011; Wise et al. 2012a). Therefore, massive star clusters consisting of Pop III stars may not form in practice. On the other hand, if metal mixing is not efficient, some pockets of pristine gas will be still able to lead to the formation of Pop III star clusters, with short core-collapse time scales (see however, Smith et al. 2015).

Local metal poor globular clusters can give constraints on the stellar IMF, density and the cluster's size to explain their old-age of $\gtrsim 10$ Gyr. Based on our results star clusters with a local IMF and initial size of $\gtrsim 1$ pc should be long-lived.

4.2 Metal poor globular clusters

Merging haloes between $M_h \sim 10^9 - 10^{10} M_\odot$ in our model result in the formation of globular clusters. We here present the mass function focusing on those with $t_{CC} > 3$ Myr and $E_{SN} > E_{grav}$. For the star clusters with $t_{CC} > 3$ Myr, central massive BH seeds via core-collapse do not form, leaving the stars unaffected in the cluster. In addition, if $E_{SN} > E_{grav}$, SN feedback is likely to suppress further gas accretion onto the star clusters, resulting in isolated systems that are dense and compact.

Figure 11 shows the mass function at $z = 6$. The mass function has a peak at $M \sim 1.5 \times 10^5 M_\odot$ and the mass range is consistent with that of observed globular clusters in local Universe. Recent observation of metal-poor globular clusters (MPGCs) show that the stellar population is very old, and compatible with formation at $z \gtrsim 6$ (Brodie & Strader 2006). We compare the number density of MPGCs in our model with that of the observed one in local Universe. Figure 12 shows the redshift evolution of MPGCs. The number density increases with decreasing redshift, and reaches $N_{GC} \sim 5 \times 10^{-7} \text{ Mpc}^{-3}$ at $z = 6$ similar to the local number density of MPGCs which is $N_{GC} \sim 1 \text{ Mpc}^{-3}$ (Barmby et al. 2000; Forbes et al. 2000). Thus, our model alone cannot reproduce the number density of the observed local MPGCs, while it matches their physical properties (size and mass).

The subsequent interaction with their environment via processes like tidal stripping and merging (e.g., Leon et al. 2000) will change the mass function of MPGCs and its final outcome will depend on the future evolution.

Recently Trenti et al. (2015) modeled local MPGCs in cosmological N-body simulations (see also Moore et al. 2006). They assumed GCs form in merging primordial haloes of $10^8 M_\odot$ at $z \sim 10$, and used their model to explain the observed nature of local MPGCs, e.g., age and metallicity distribution, and their spacial distribution. Our model of GC formation requires somewhat more massive merging haloes ($\gtrsim 10^9 M_\odot$) suggesting a possible halo mass bias leading to the formation of black hole seeds.

5 SUMMARY

In this work, we analytically model the formation of MBHs in the first merging galaxies. These BHs provide the natural seeds for SMBH at $z \sim 6$. We show that compact star

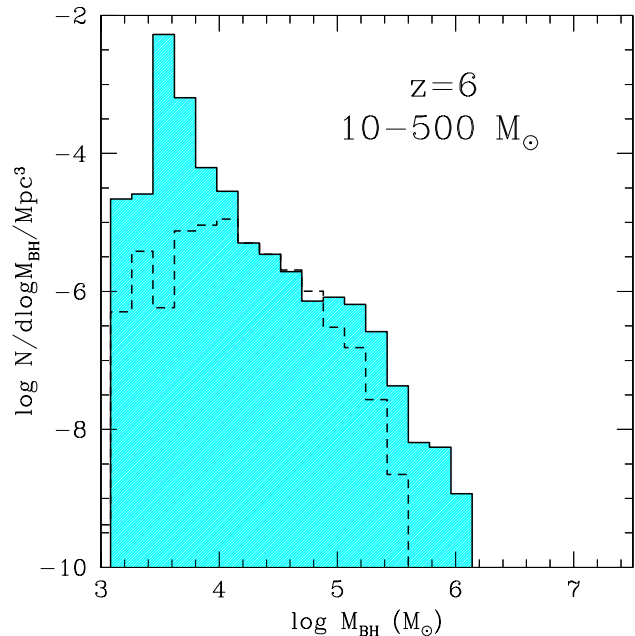


Figure 10. Black hole mass function at $z = 6$ assuming a top heavy IMF in the mass ranges 10 to 500 M_{\odot} with slope $\alpha = -2.35$. Dash lines show our fiducial model ($M = 0.1 - 100 M_{\odot}$) as shown in Figure 8.

clusters that likely form during such mergers are prone to core-collapse and produce VMSs of $\sim 1000 M_{\odot}$ at their centres. VMSs collapse to BHs without going through a SN stage and subsequently grow via swallowing stars in their vicinity. Relaxation processes are efficient in refilling the loss cone around the BH continuously with new stars. We find that the BHs mass sensitively depends on the the radius and mass of the hosting star clusters which determine the core-collapse and stellar relaxation time scales. Within this scenario major mergers of galaxies with $\gtrsim 4 \times 10^8 M_{\odot}$ at $z \sim 20$ lead to the formation of $\gtrsim 10^5 M_{\odot}$ BHs by $z \sim 10$ which are likely progenitors of SMBHs at $z \gtrsim 6$.

Based on our results the average relation between host stellar mass and black hole mass will not be the same as observed in the local universe. Such deviation will reduce over time as merging of galaxies and black holes will move host galaxies and black holes closer to the locally observed relation as a consequence of the central limit theorem (Peng 2007; Hirschmann et al. 2010).

Our model predictions are sensitive to the properties of the hosting star clusters, e.g., mass, radius, IMF of stars. We here assumed physically motivated analytic relations that we will further test and systematically investigate in a follow-up study using detailed numerical simulations.

ACKNOWLEDGMENTS

We are grateful to N. Yoshida and A. Ferrara for valuable discussion.

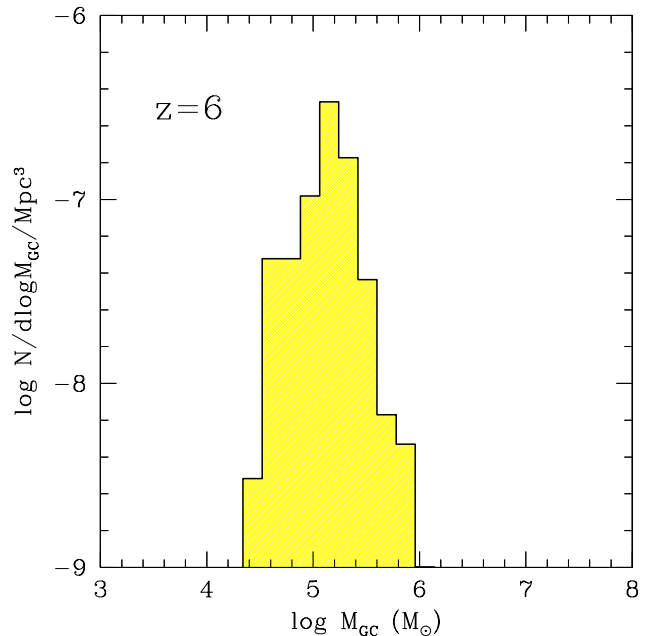


Figure 11. Mass function of globular clusters resulting from mergers of galaxies.

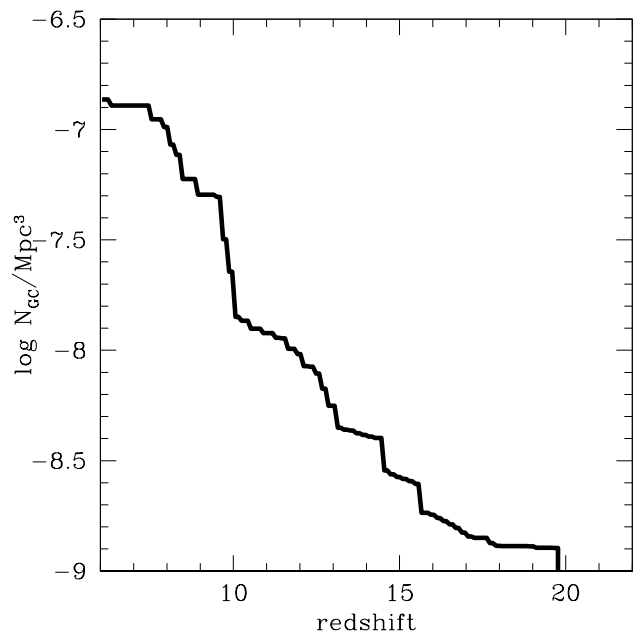


Figure 12. Redshift evolution of the number density of globular clusters.

REFERENCES

- Abel T., Bryan G. L., Norman M. L., 2002, *Science*, 295, 93
- Agarwal B., Dalla Vecchia C., Johnson J. L., Khochfar S., Paardekooper J.-P., 2014, *MNRAS*, 443, 648
- Agarwal B., Davis A. J., Khochfar S., Natarajan P., Dunlop J. S., 2013, *MNRAS*, 432, 3438

- Agarwal B., Khochfar S., 2015, *MNRAS*, 446, 160
- Agarwal B., Khochfar S., Johnson J. L., Neistein E., Dalla Vecchia C., Livio M., 2012, *MNRAS*, 425, 2854
- Alvarez M. A., Wise J. H., Abel T., 2009, *ApJ*, 701, L133
- Barmby P., Huchra J. P., Brodie J. P., Forbes D. A., Schroder L. L., Grillmair C. J., 2000, *AJ*, 119, 727
- Barnes J. E., Hernquist L., 1996, *ApJ*, 471, 115
- Begelman M. C., Volonteri M., Rees M. J., 2006, *MNRAS*, 370, 289
- Binney J., Tremaine S., 2008, *Galactic Dynamics: Second Edition*. Princeton University Press
- Booth C. M., Schaye J., 2009, *MNRAS*, 398, 53
- Brodie J. P., Strader J., 2006, *ARA&A*, 44, 193
- Bromm V., Coppi P. S., Larson R. B., 2002, *ApJ*, 564, 23
- Bromm V., Loeb A., 2003, *ApJ*, 596, 34
- Chen X., Liu F. K., 2013, *ApJ*, 762, 95
- Choi J.-H., Shlosman I., Begelman M. C., 2013, *ApJ*, 774, 149
- Clark P. C., Glover S. C. O., Smith R. J., Greif T. H., Klessen R. S., Bromm V., 2011, *Science*, 331, 1040
- Cox T. J., Dutta S. N., Di Matteo T., Hernquist L., Hopkins P. F., Robertson B., Springel V., 2006, *ApJ*, 650, 791
- Devecchi B., Volonteri M., Colpi M., Haardt F., 2010, *MNRAS*, 409, 1057
- Di Matteo T., Colberg J., Springel V., Hernquist L., Sijacki D., 2008, *ApJ*, 676, 33
- Di Matteo T., Khandai N., DeGraf C., Feng Y., Croft R. A. C., Lopez J., Springel V., 2012, *ApJ*, 745, L29
- Di Matteo T., Springel V., Hernquist L., 2005, *Nature*, 433, 604
- Dijkstra M., Haiman Z., Mesinger A., Wyithe J. S. B., 2008, *MNRAS*, 391, 1961
- Fan X., Strauss M. A., Becker R. H., White R. L., Gunn J. E., Knapp G. R., Richards G. T., Schneider D. P., Brinkmann J., Fukugita M., 2006, *AJ*, 132, 117
- Fan X., et al., 2001, *AJ*, 122, 2833
- Ferrara A., Haardt F., Salvaterra R., 2013, *MNRAS*, 434, 2600
- Forbes D. A., Masters K. L., Minniti D., Barmby P., 2000, *A&A*, 358, 471
- Fujii M. S., Portegies Zwart S., 2014, *MNRAS*, 439, 1003
- Gültekin K., Richstone D. O., Gebhardt K., Lauer T. R., Tremaine S., Aller M. C., Bender R., Dressler A., Faber S. M., Filippenko A. V., Green R., Ho L. C., Kormendy J., Magorrian J., Pinkney J., Siopis C., 2009, *ApJ*, 698, 198
- Heger A., Fryer C. L., Woosley S. E., Langer N., Hartmann D. H., 2003, *ApJ*, 591, 288
- Heger A., Woosley S. E., 2002, *ApJ*, 567, 532
- Hirano S., Hosokawa T., Yoshida N., Umeda H., Omukai K., Chiaki G., Yorke H. W., 2014, *ApJ*, 781, 60
- Hirschmann M., Khochfar S., Burkert A., Naab T., Genel S., Somerville R. S., 2010, *MNRAS*, 407, 1016
- Hopkins P. F., Cox T. J., Younger J. D., Hernquist L., 2009, *ApJ*, 691, 1168
- Hopkins P. F., Hernquist L., Cox T. J., Di Matteo T., Robertson B., Springel V., 2006, *ApJS*, 163, 1
- Hopman C., Alexander T., 2006, *ApJ*, 645, 1152
- Hosokawa T., Yorke H. W., Inayoshi K., Omukai K., Yoshida N., 2013, *ApJ*, 778, 178
- Inayoshi K., Omukai K., 2012, *MNRAS*, 422, 2539
- Inayoshi K., Omukai K., Tasker E., 2014, *MNRAS*, 445, L109
- Inayoshi K., Tanaka T. L., 2014, *ArXiv e-prints*
- Inayoshi K., Visbal E., Kashiyama K., 2015, *ArXiv e-prints*
- Johnson J. L., Dalla V. C., Khochfar S., 2013, *MNRAS*, 428, 1857
- Johnson J. L., Khochfar S., 2011, *ApJ*, 743, 126
- Johnson J. L., Whalen D. J., Agarwal B., Paardekoope J.-P., Khochfar S., 2014, *MNRAS*, 445, 686
- Katz H., Sijacki D., Haehnelt M. G., 2015, *MNRAS*, 451, 2352
- Khochfar S., Silk J., 2009, *MNRAS*, 397, 506
- , 2011, *MNRAS*, 410, L42
- Kocsis B., Tremaine S., 2011, *MNRAS*, 412, 187
- Kormendy J., Ho L. C., 2013, *ARA&A*, 51, 511
- Krumholz M. R., Dekel A., McKee C. F., 2012, *ApJ*, 745, 69
- Lacey C., Cole S., 1993, *MNRAS*, 262, 627
- Latif M. A., Schleicher D. R. G., Schmidt W., Niemeyer J. C., 2013, *MNRAS*, 436, 2989
- Leon S., Meylan G., Combes F., 2000, *A&A*, 359, 907
- Li Y., Hernquist L., Robertson B., Cox T. J., Hopkins P. F., Springel V., Gao L., Di Matteo T., Zentner A. R., Jenkins A., Yoshida N., 2007, *ApJ*, 665, 187
- Lodato G., Natarajan P., 2006, *MNRAS*, 371, 1813
- , 2007, *MNRAS*, 377, L64
- Maio U., Khochfar S., Johnson J. L., Ciardi B., 2011, *MNRAS*, 414, 1145
- Marconi A., Hunt L. K., 2003, *ApJ*, 589, L21
- Mayer L., Kazantzidis S., Escala A., Callegari S., 2010, *Nature*, 466, 1082
- Milosavljević M., Bromm V., Couch S. M., Oh S. P., 2009a, *ApJ*, 698, 766
- Milosavljević M., Couch S. M., Bromm V., 2009b, *ApJ*, 696, L146
- Mo H. J., Mao S., White S. D. M., 1998, *MNRAS*, 295, 319
- Moore B., Diemand J., Madau P., Zemp M., Stadel J., 2006, *MNRAS*, 368, 563
- Mortlock D. J., Warren S. J., Venemans B. P., Patel M., Hewett P. C., McMahon R. G., Simpson C., Theuns T., Gonz  les-Solares E. A., Adamson A., Dye S., Hambly N. C., Hirst P., Irwin M. J., Kuiper E., Lawrence A., R  tgering H. J. A., 2011, *Nature*, 474, 616
- Naab T., Khochfar S., Burkert A., 2006, *ApJ*, 636, L81
- Nakamura F., Umemura M., 2001, *ApJ*, 548, 19
- Oesch P. A., Bouwens R. J., Illingworth G. D., Labb   I., Smit R., Franx M., van Dokkum P. G., Momcheva I., Ashby M. L. N., Fazio G. G., Huang J.-S., Willner S. P., Gonzalez V., Magee D., Trenti M., Brammer G. B., Skelton R. E., Spitler L. R., 2014, *ApJ*, 786, 108
- Omukai K., Nishi R., 1998, *ApJ*, 508, 141
- Omukai K., Palla F., 2003, *ApJ*, 589, 677
- Omukai K., Schneider R., Haiman Z., 2008, *ApJ*, 686, 801
- Omukai K., Tsuribe T., Schneider R., Ferrara A., 2005, *ApJ*, 626, 627
- Paardekooper J.-P., Khochfar S., Dalla Vecchia C., 2013, *MNRAS*, 429, L94
- Park K., Ricotti M., 2011, *ApJ*, 739, 2
- , 2012, *ApJ*, 747, 9
- Peng C. Y., 2007, *ApJ*, 671, 1098
- Portegies Zwart S. F., McMillan S. L. W., 2002, *ApJ*, 576, 899

- Rauch K. P., Tremaine S., 1996, *New Astron.*, 1, 149
- Rees M. J., 1978, *The Observatory*, 98, 210
- Regan J. A., Haehnelt M. G., 2009, *MNRAS*, 396, 343
- Regan J. A., Johansson P. H., Haehnelt M. G., 2014, *MNRAS*, 439, 1160
- Smith B., Wise J., O’Shea B., Norman M., Khochfar S., 2015, *ArXiv e-prints*
- Somerville R. S., Kolatt T. S., 1999, *MNRAS*, 305, 1
- Spaans M., Silk J., 2006, *ApJ*, 652, 902
- Springel V., Di Matteo T., Hernquist L., 2005, *ApJL*, 620, L79
- Stacy A., Greif T. H., Bromm V., 2010, *MNRAS*, 403, 45
- , 2012, *MNRAS*, 422, 290
- Stark D. P., Schenker M. A., Ellis R., Robertson B., McLure R., Dunlop J., 2013, *ApJ*, 763, 129
- Sugimura K., Omukai K., Inoue A. K., 2014, *MNRAS*, 445, 544
- Susa H., 2013, *ApJ*, 773, 185
- Susa H., Hasegawa K., Tominaga N., 2014, *ApJ*, 792, 32
- Trenti M., Padoan P., Jimenez R., 2015, *ArXiv e-prints*
- Turk M. J., Abel T., O’Shea B., 2009, *Science*, 325, 601
- Umemura M., Susa H., Hasegawa K., Suwa T., Semelin B., 2012, *Progress of Theoretical and Experimental Physics*, 2012, 010000
- van den Bosch F. C., 2001, *MNRAS*, 327, 1334
- Wise J. H., Abel T., Turk M. J., Norman M. L., Smith B. D., 2012a, *MNRAS*, 427, 311
- Wise J. H., Turk M. J., Norman M. L., Abel T., 2012b, *ApJ*, 745, 50
- Wu X.-B., Wang F., Fan X., Yi W., Zuo W., Bian F., Jiang L., McGreer I. D., Wang R., Yang J., Yang Q., Thompson D., Beletsky Y., 2015, *Nature*, 518, 512
- Yoshida N., Omukai K., Hernquist L., 2008, *Science*, 321, 669
- Yoshida N., Omukai K., Hernquist L., Abel T., 2006, *ApJ*, 652, 6